REPORT DOCUMENTATION PAGE

Form Approved
OMB No. 0704-0188

1. REPORT DATE (DD-MM-YYYY)	2. REPORT TYPE	3. DATES COVERED (From - To)
29-Sep-2006	REPRINT	

4. TITLE AND SUBTITLE
ANALYSIS OF SHEAR WAVE GENERATION BY DECOUPLED AND PARTIALLY COUPLED EXPLOSIONS

5a. CONTRACT NUMBER
FA8718-06-C-0007

5b. GRANT NUMBER

5c. PROGRAM ELEMENT NUMBER
62601F

6. AUTHOR(S)
Jeffry L. Stevens, Heming Xu, and G. Eli Baker

5d. PROJECT NUMBER
1010

5e. TASK NUMBER
SM

5f. WORK UNIT NUMBER
A1

7. PERFORMING ORGANIZATION NAME(S) AND ADDRESS(ES)

Science Applications International Corporation
10260 Campus Point Drive
San Diego, CA 92121-1152

8. PERFORMING ORGANIZATION REPORT NUMBER

9. SPONSORING / MONITORING AGENCY NAME(S) AND ADDRESS(ES)
Air Force Research Laboratory
29 Randolph Road
Hanscom AFB, MA 01731-3010

10. SPONSOR/MONITOR'S ACRONYM(S)
AFRL/VSBYE

11. SPONSOR/MONITOR'S REPORT NUMBER(S)
AFRL-VS-HA-TR-2006-1113

12. DISTRIBUTION / AVAILABILITY STATEMENT
Approved for Public Release; Distribution Unlimited.

13. SUPPLEMENTARY NOTES
Reprinted from: Proceedings of the 28th Seismic Research Review – Ground-Based Nuclear Explosion Monitoring Technologies, 19 – 21 September 2006, Orlando, FL, Volume I pp 693 - 703.

14. ABSTRACT

The objective of this new project is to investigate the sources of shear wave generation by decoupled and partially coupled explosions, and the differences in shear wave generation between tamped and decoupled explosions, using data analysis and numerical modeling of decoupled and partially coupled explosions.

During the first phase of this project, we focused on three theoretical mechanisms for generation of shear waves from decoupled and partially coupled explosions. The first mechanism is offset of the explosion from the center of the cavity, causing impact on the sides to vary in both amplitude and time. We worked out the general solution to this problem, and then performed calculations of an airshock propagating in the cavity and impacting the cavity wall. We find that the offset explosion acts like a dipole source and can generate significant shear waves with a modest offset from the center. The second physical mechanism is an explosion in an aspherical cavity, in this case a cylindrical tunnel.

The third physical mechanism we considered is crack growth outside of a partially coupled explosion. We are investigating two types of crack distributions: (1) small hydrofractures distributed broadly around the explosion in response to tensile stresses and (2) generation of a smaller number of larger hydrofractures. We are performing these calculations using the nonlinear axisymmetric finite difference code CRAM, with crack propagation algorithms developed by Nilson et al. (1991). We use the representation theorem to calculate outgoing P and S waves to determine the additional S waves generated by the cracks.

To complement these calculations, we are examining existing records of and reports on historical decoupled explosions, in particular, data from Khirgizhia decoupling experiments and Azgir decoupled nuclear explosions in the former Soviet Union, the U.S. Salmon/Sterling experiment, and extensive reports on the British Orpheus decoupling experiments. A consistent result between all data sets for which such data is available is that at low frequencies (<~2 Hz) local records of collocated tamped and decoupled explosions scaled for yield have significant and identical shear waves. At higher frequencies (~5–15 Hz), however the tamped explosions generate larger shear waves than the collocated decoupled explosions. Near field records of the decoupled explosion Sterling are found to have strong shear waves at frequencies above 20 Hz, while the records show pure radial P-wave motion at lower frequencies. In contrast, records at similar ranges for Salmon show pure radial P-wave motion at all frequencies. We are in the process of performing two-dimensional axisymmetric finite difference calculations of the Salmon and Sterling explosions. The Salmon calculation has been completed and provides an excellent match to the near field data.

15. SUBJECT TERMS
Seismic characterization, Seismic propagation

16. SECURITY CLASSIFICATION OF:			17. LIMITATION OF ABSTRACT	18. NUMBER OF PAGES	19a. NAME OF RESPONSIBLE PERSON
a. REPORT	b. ABSTRACT	c. THIS PAGE			Robert J. Raistrick
UNCLAS	UNCLAS	UNCLAS	SAR	11	19b. TELEPHONE NUMBER (include area code) 781-377-3726

ANALYSIS OF SHEAR WAVE GENERATION BY DECOUPLED AND PARTIALLY COUPLED EXPLOSIONS

Jeffry L. Stevens, Heming Xu, and G. Eli Baker

Science Applications International Corporation

Sponsored by Air Force Research Laboratory

Contract No. FA8718-06-C-0007

ABSTRACT

The objective of this new project is to investigate the sources of shear wave generation by decoupled and partially coupled explosions, and the differences in shear wave generation between tamped and decoupled explosions, using data analysis and numerical modeling of decoupled and partially coupled explosions.

During the first phase of this project, we focused on three theoretical mechanisms for generation of shear waves from decoupled and partially coupled explosions. The first mechanism is offset of the explosion from the center of the cavity, causing impact on the sides to vary in both amplitude and time. We worked out the general solution to this problem, and then performed calculations of an airshock propagating in the cavity and impacting the cavity wall. We find that the offset explosion acts like a dipole source and can generate significant shear waves with a modest offset from the center. The second physical mechanism is an explosion in an aspherical cavity, in this case a cylindrical tunnel.

The third physical mechanism we considered is crack growth outside of a partially coupled explosion. We are investigating two types of crack distributions: (1) small hydrofractures distributed broadly around the explosion in response to tensile stresses and (2) generation of a smaller number of larger hydrofractures. We are performing these calculations using the nonlinear axisymmetric finite difference code CRAM, with crack propagation algorithms developed by Nilson et al. (1991). We use the representation theorem to calculate outgoing P and S waves to determine the additional S waves generated by the cracks.

To complement these calculations, we are examining existing records of and reports on historical decoupled explosions, in particular, data from Khirgizhia decoupling experiments and Azgir decoupled nuclear explosions in the former Soviet Union, the U.S. Salmon/Sterling experiment, and extensive reports on the British Orpheus decoupling experiments. A consistent result between all data sets for which such data is available is that at low frequencies (<~2 Hz) local records of collocated tamped and decoupled explosions scaled for yield have significant and identical shear waves. At higher frequencies (~5–15 Hz), however the tamped explosions generate larger shear waves than the collocated decoupled explosions. Near field records of the decoupled explosion Sterling are found to have strong shear waves at frequencies above 20 Hz, while the records show pure radial P-wave motion at lower frequencies. In contrast, records at similar ranges for Salmon show pure radial P-wave motion at all frequencies. We are in the process of performing two-dimensional axisymmetric finite difference calculations of the Salmon and Sterling explosions. The Salmon calculation has been completed and provides an excellent match to the near field data.

OBJECTIVES

The objective of this project is to investigate the sources of shear wave generation by decoupled and partially coupled explosions, and the differences in shear wave generation between tamped and decoupled explosions. This is being accomplished through a program of data analysis and numerical modeling of decoupled and partially coupled explosions.

RESEARCH ACCOMPLISHED

Introduction

Detonation of a nuclear explosion in a large cavity to decouple the source from the surrounding medium and so evade detection has been a concern for nuclear monitoring for many decades (e.g., Latter et al., 1961). Most previous work on decoupling has focused on the empirical evaluation and numerical modeling of frequency dependent decoupling of explosions in cavities to address evasion. The "decoupling factor," which is the amplitude ratio of the seismic signals of the tamped to the decoupled explosions, depends on the emplacement media, but can be as large as two orders of magnitude. Consequently while decoupled explosions of less than a kiloton may be detected by a capable seismic network, the seismic signal is small enough that it may be difficult to distinguish from the large number of small earthquakes and mining explosions that occur in the same magnitude range ($< \sim 2.5$). Discrimination of decoupled explosions from this background noise is therefore an important issue.

The most reliable discriminants for events in the magnitude range of decoupled explosions are high frequency spectral ratios of the amplitudes of the seismic shear phases Sn and Lg to Pn or Pg, with explosions in general having lower S/P ratios than earthquakes. It is therefore very important to understand the shear wave generation by decoupled and partially coupled explosions in order to ensure that they are identified correctly by the discriminants that depend on shear wave amplitudes, and to identify any circumstances under which the discriminants could fail.

At first glance, generation of shear waves by a decoupled explosion might appear to be an easy problem, since a nuclear explosion detonated at the center of a perfect spherical cavity large enough to decouple the explosion would generate no shear waves (other than conversions due to the earth's surface and scattering). However, there are several problems with this simple picture:

1. shear waves have been observed from all decoupled explosions, even quite close to the source;
2. no cavity actually has perfect spherical symmetry; and
3. partially coupled explosions generate cracks more readily than tamped explosions.

Our research program follows these three points. First, we review existing data for decoupled and partially coupled nuclear explosions. As pointed out above, this data has been extensively studied to understand decoupling, but much less has been done with the shear wave data. We find that there is one consistent difference between data from tamped and decoupled explosions: S/P ratios at high frequencies are larger for tamped explosions than for decoupled explosions. This is not the case at lower frequencies, where S/P ratios are observed to be nearly identical for tamped and decoupled explosions. This puts some constraints on shear wave generation mechanisms that may be operating in each case. Second, we model shear waves generated by explosions with two types of source asymmetry: non-spherical cavities and offset or asymmetric explosion sources. Our particular interest is in determining how much asymmetry is necessary to generate significant shear waves. We investigate this in two ways: (1) using nonlinear calculations of an explosion source in a non-spherical cavity and (2) using a modification of the method of Stevens (1980) to predict non-spherical oscillations of the cavity due to asymmetries in the incident stress field. Third, we model seismic waves caused by cracks generated by partially coupled explosions. Such cracks could substantially increase the shear waves generated by the explosion, complicating the discrimination problem. Finally, we are performing full two-dimensional axisymmetric finite difference calculations of the Salmon and Sterling explosions in order to understand the shear waves generated by those two important events.

Observed Frequency Dependent Differences in Shear Waves between Decoupled and Tamped Explosions

Recordings on the same instruments, from co-located tamped and decoupled explosions, normalized by the P wave to account for absolute amplitude differences due to yield and decoupling, have nearly identical shear waveforms below 2 Hz, but have relatively more S with increasing frequency. Figure 1 shows such records for Salmon, a tamped 5.3 kt nuclear explosion at 828 m depth in salt, and Sterling, the 0.38 kt nuclear explosion detonated in Salmon's 17 m radius cavity. Figure 2 is similar, but for a 64 kt tamped Azgir nuclear explosion at 987 m depth in salt and the 10 kt nuclear explosion detonated in the first explosion's 38 m horizontal radius by 33 m vertical radius cavity. Figure 3 shows records at 5 km from adjacent one ton decoupled (red) and tamped (blue) chemical explosions in limestone in Kirghizia. The decoupled explosion was suspended in a 4.92 m radius cavity.

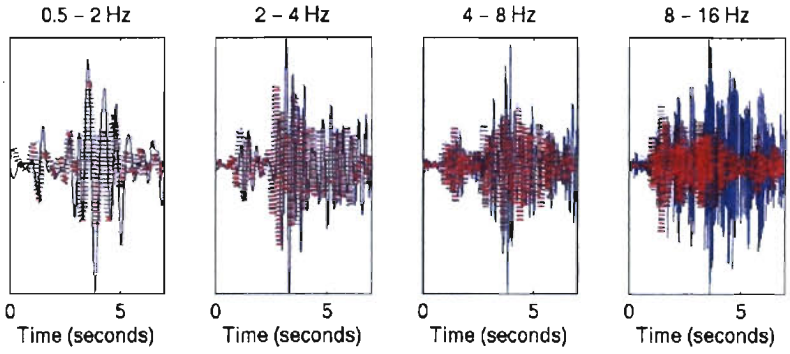

Figure 1. Salmon (blue) and Sterling (red, dotted) vertical records at 16 km, scaled by the first second of P.

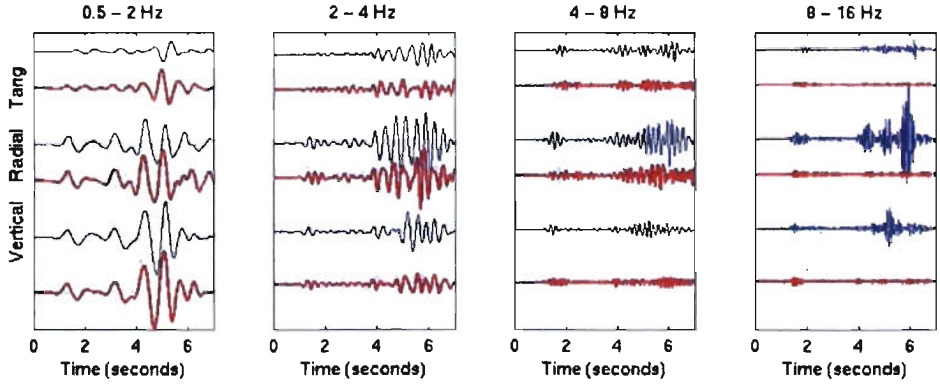

Figure 2. Tangential (upper 2 traces), radial (middle 2 traces), and vertical (bottom 2 traces) records at 18 km for tamped (blue) and decoupled (red) Azgir nuclear explosions in 4 passbands, scaled by the vertical P-wave rms amplitude. Time relative to origin is unknown. Initial P arrival is set at 1 s.

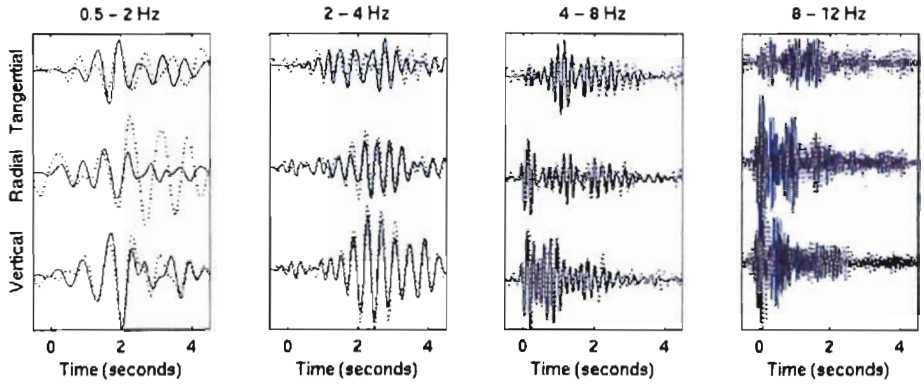

Figure 3. Tangential, radial, and vertical (top to bottom) seismograms 5 km from one ton decoupled (red) and tamped (blue) explosions, scaled by the vertical P amplitude. All three components for each event are on the same scale. Time is from the initial P arrival. SV arrives ~0.5 s after P.

Shear Waves from a Non-Isotropic Explosion Source

Stevens (1980) developed a solution for the seismic waves generated by an explosion in an arbitrarily prestressed elastic medium. Here we generalize the solution to allow for cases where the explosion is non-isotropic. In particular, we consider cases where the explosion is offset from the center of the cavity so that the amplitude and arrival time of the explosion vary as a function of position on the cavity wall. The general solution for the seismic wave field from a set of tractions applied to the inside of a spherical cavity is given by

$$u = -\int_{\Sigma} u \cdot T(G) \cdot \hat{n} dA + \int_{\Sigma} G \cdot T(u) \cdot \hat{n} dA - \frac{1}{i\omega} \int_{\Sigma} G \cdot T(u^*) \cdot \hat{n} dA \,, \tag{1}$$

where Σ is the cavity surface, u on the left side of the equation is the displacement at any location outside the cavity, and u inside the integral is the displacement on the cavity wall. G is the elastic Green's tensor in spherical coordinates, and T is the stress operator; u^* is the difference in the static displacement field before and after the explosion due to changes in the static stress field, and so will vanish for a decoupled explosion where the prestress does not change, but will be non-zero for a tamped explosion with tectonic strain release. The third integral therefore represents the response of the medium to a change in prestress, the second term represents the response of the medium to the applied stress from the explosion, and the first term represents the additional motion due to the response of the cavity wall.

Equation 1 can be solved by expanding the displacement, traction and Green's tensor in vector spherical harmonics. The case of interest here is shown in Figure 4 (left), where the explosion source is initially offset from the center of an air-filled cavity of radius R by a distance d. The right side of Figure 4 shows the calculated P and S waves from the explosion. The offset from the center causes the shock wave to impact the side of the cavity closest to the explosion earlier and with greater force than the opposite side of a cavity. This is equivalent to a dipole source acting in the direction of the offset, and as illustrated, can generate S waves comparable in amplitude to the initial P wave.

Note that the offset in origin breaks the symmetry of the problem except for axisymmetry about the offset axis. If the offset is oriented horizontally relative to the surface, strong SH waves will be generated. Zhou and Harkrider (1992) similarly found that a point explosion offset from the center in a solid-filled spherical region embedded in a whole space acts primarily as a dipole source.

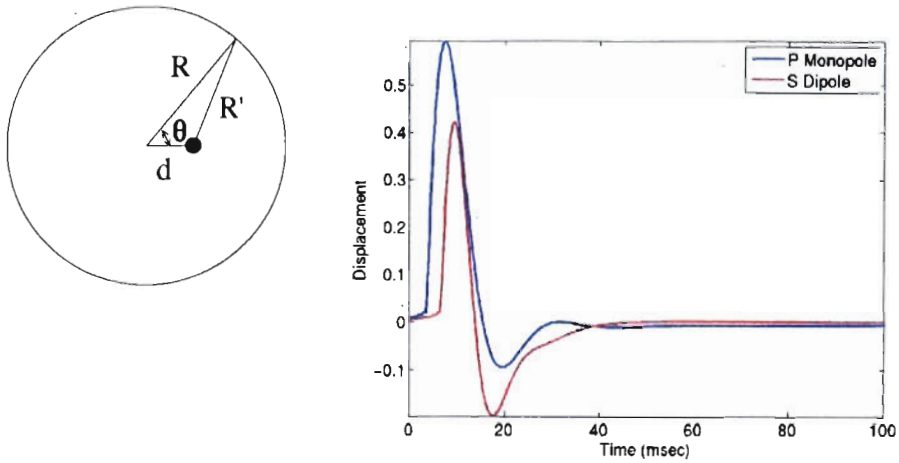

Figure 4. Calculated P and S waves (right) for an explosion in an air-filled cavity with the origin of the explosion offset from the center (left). In this example the cavity radius is 17 m and the offset from the center is 8.5 m.

Shear Waves from an Explosion in a Tunnel

Shear waves from an explosion in a tunnel are calculated using the procedure described by Rimer et al. (1994). The axisymmetric Eulerian finite difference code STELLAR is used to calculate the propagation of the air shock in the cylindrical tunnel. Just before the air shock impacts the end of the tunnel, the solution is overlaid onto a new grid that is used by the axisymmetric Lagrangian finite difference code CRAM. The calculation continues in CRAM until it reaches the linear elastic region. The representation theorem is then used to propagate the solution to the far field. In this example, we show a calculation of a 1.52 kt explosion in a cylindrical tunnel in granite with a length of 220 m and a radius of 5.4 m. Figure 5 shows the pressure field in the STELLAR computational grid at 6.6 ms and the velocity field in the CRAM grid at 10 ms.

Far-field body waves were calculated using the representation theorem to integrate the displacements and stresses on the monitoring surface together with a far-field body wave Green's function. Both P and S waves were calculated by integrating with the appropriate Green's function. Figure 6 shows the P and S waves both calculated at a 45 degree takeoff angle. The takeoff angle is measured with respect to the long axis of the cylinder, so zero is in the direction of the axis and 90 degrees is perpendicular to the long axis. S waves are largest at 45 degrees and are about ½ the amplitude of the P wave at the same takeoff angle.

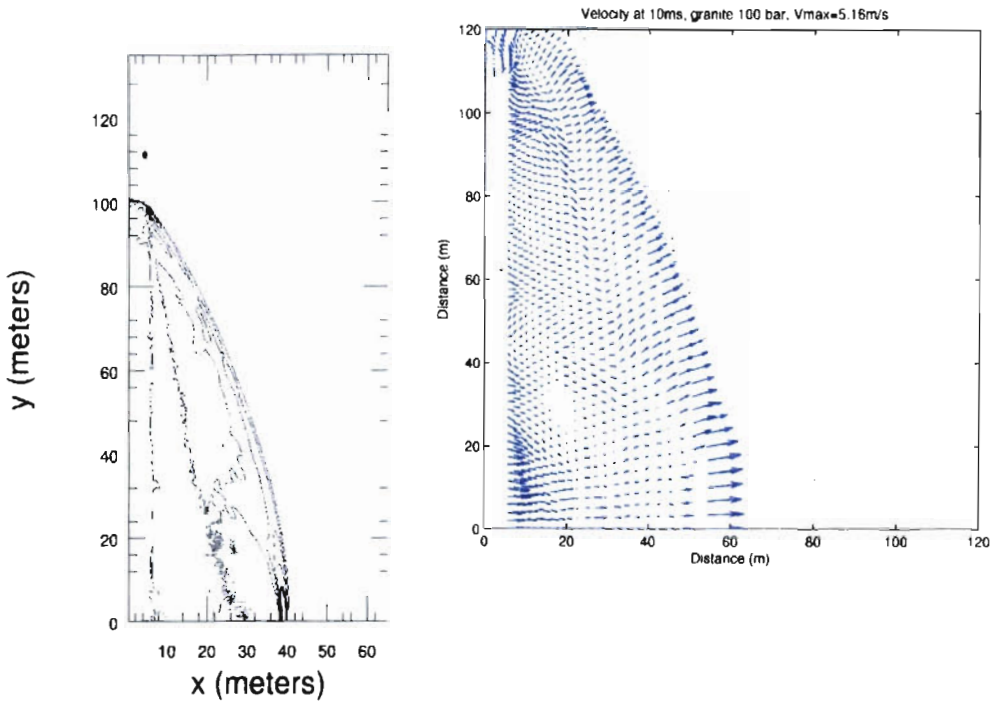

Figure 5. Pressure contours from STELLAR calculation (left) at the overlay time of 6.6 ms, and velocity field from CRAM calculation (right) at 10 ms. Only ¼ of the computed fields are shown because of symmetry about the y=0 plane and the axisymmetric x=0 line.

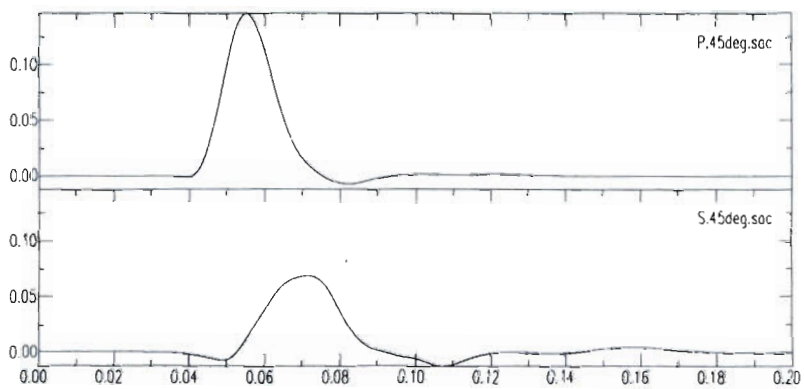

Figure 6. Far-field P (top) and S (bottom) displacement for the tunnel calculation at a takeoff angle of 45 degrees. Waveforms were lowpass filtered at 40 Hz.

Shear Waves from Hydrofractures

Crack generation has long been a concern for containment of underground nuclear explosions. During the nuclear testing program considerable effort was expended on prediction of crack generation and propagation during explosions. One of the programs developed for this purpose as part of the containment program is F-Cubed (Nilson et al., 1991). F-Cubed combines the CRAM Lagrangian finite difference code with the FAST fracture propagation code, and can predict crack generation and propagation outside of tamped or partially coupled explosions. It can be used in either of two ways: (1) to predict where cracks will occur and (2) to predict the opening and propagation of known cracks or cracks along suspected zones of weakness. Here we use it to predict crack generation.

Nonlinear stress wave dynamics of rock are affected by the penetration of gases into fractures, which fragments the rock and changes the burden. We model the interaction between stress waves and fully-pressurized fractures by assuming that the pressure within the crack is everywhere equal to the instantaneous cavity pressure. The growth of a swarm of hydrofractures is calculated by allowing the fluid to enter any computational cell having a minimum compressive stress less than the cavity pressure, subject to the connectivity, angular orientation and propagation speed restrictions. The following figures compare the characteristics of wave generation in a Nevada Test Site (NTS) structure with and without hydrofracturing. The partially coupled explosion has an initial cavity radius of 10 m, and an explosion yield such that the vaporization radius is also approximately 10 m. Although this is almost large enough to be considered tamped, the air-filled cavity makes it more subject to cracking than a fully tamped explosion. Figures 7–11 illustrate the effects of a swarm of hydrofractures on the far field seismogram and the compressional and shear waves. Figure 11 shows amplification of the S and higher mode surface waves relative to P and the fundamental mode surface wave.

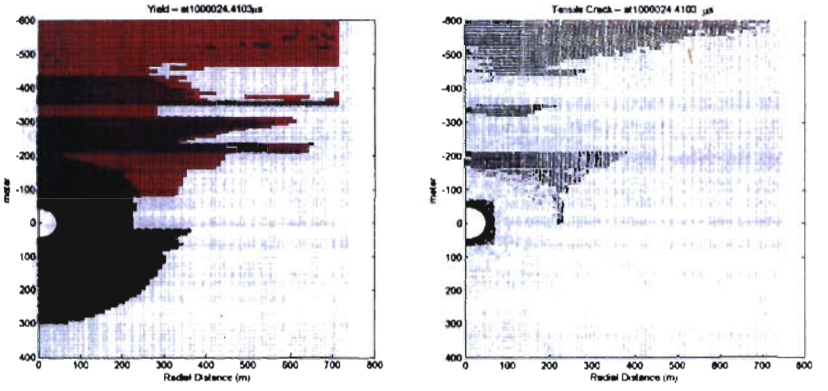

Figure 7. Yield and tensile cracks in the absence of hydrofracturing. The left panel shows the yield extent at 1 s and the right shows the tensile crack distribution.

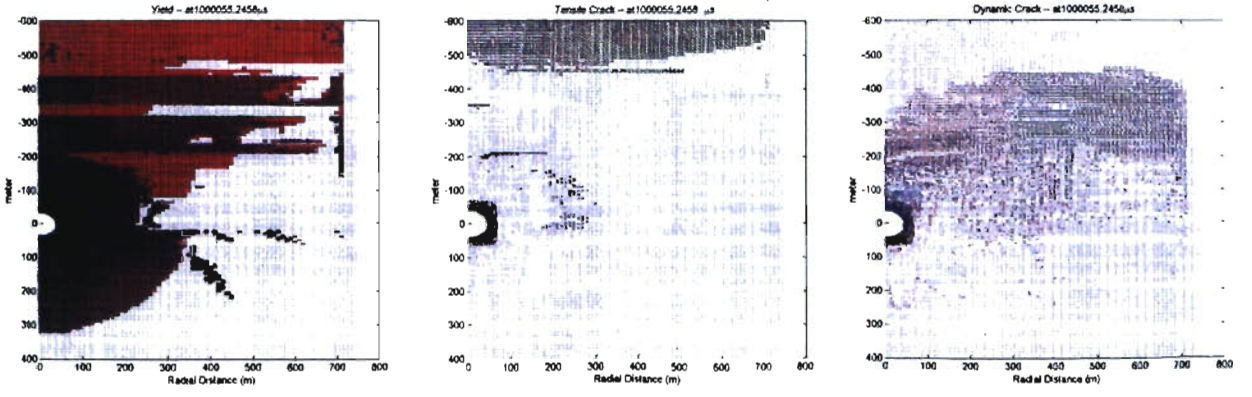

Figure 8. Yield (left), tensile cracks (middle) and hydrofractures (right) from a calculation including prediction of hydrofractures.

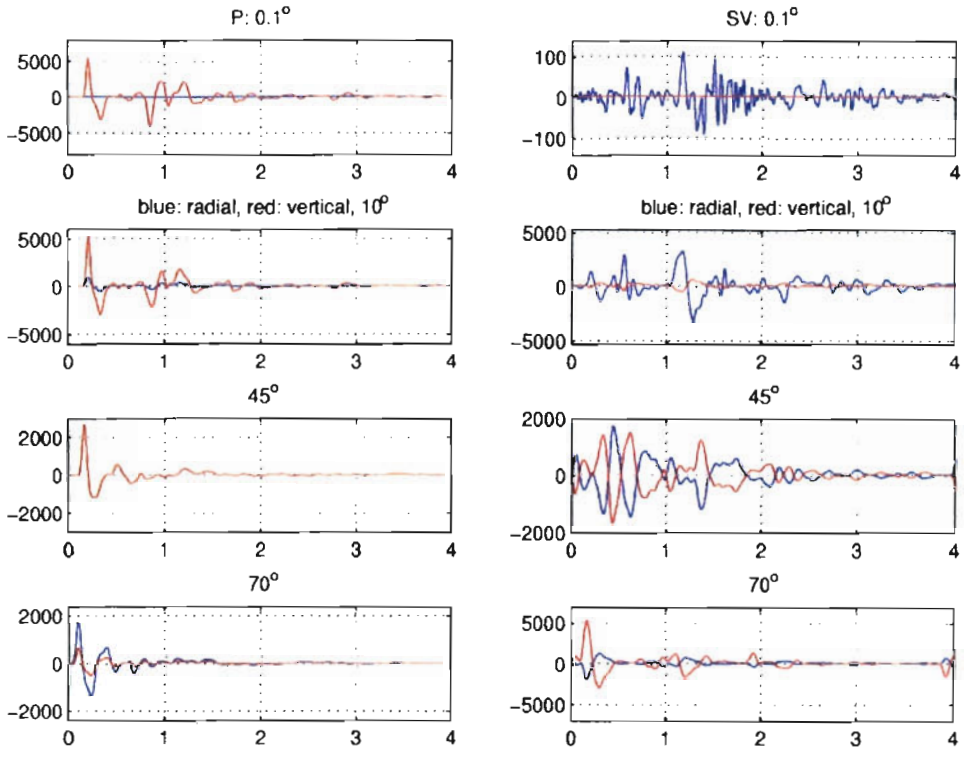

Figure 9. Body waves in the absence of hydrofracturing. The left panel shows the compressional body waves at different take-off angles and the right shows the shear waves. The red lines denote the vertical component and the blue lines the radial component.

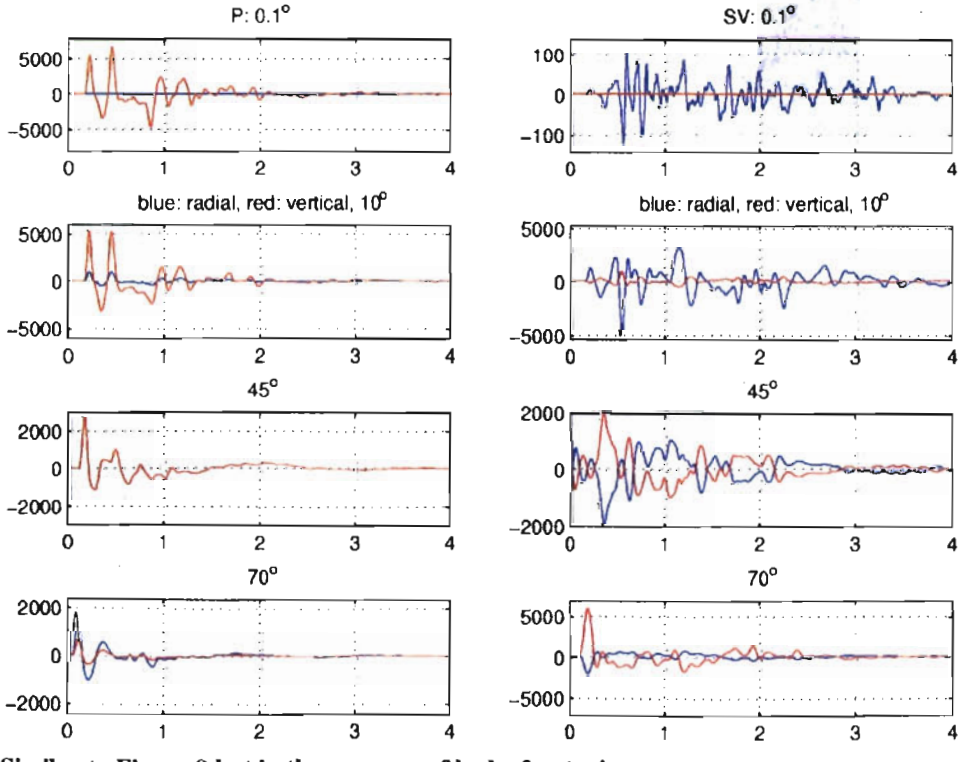

Figure 10. Similar to Figure 9 but in the presence of hydrofracturing.

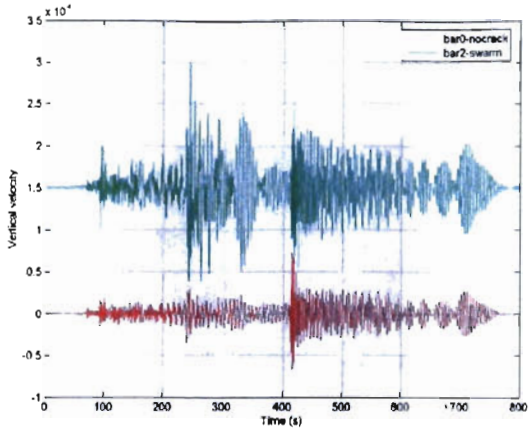

Figure 11. Comparison of seismograms at 500 km with and without hydrofracturing. The green line represents the seismogram in the presence of hydrofracturing.

Salmon/Sterling Axisymmetric Calculations

Salmon was a tamped 5.3 kt nuclear explosion detonated at 828 m depth in the Tatum salt dome. Rimer and Cherry (1982) successfully modeled the explosion event in the spherical case and found that ground motion data were best modeled by using the salt work-softening-hardening model, which is required in order to explain the small amplitude "elastic" precursor which is inconsistent with the laboratory strength measurements. The implementation in the finite-difference method is to calculate the strength as a function of the inelastic energy deposited in the material during yielding, i.e., $(Y = Y_0(1 + e_1 E - e_2 E^2) \le Y_{Lim})$, where Y_0 is the initial strength and e_1 and e_2 are respectively work hardening and work softening material constants.

We use the same parameters obtained in the spherical case to model the Salmon explosion in cylindrical symmetry with four layers (sediment, limestone, anhydrite and salt, see Murphy, 1991) and a free surface. The calculated final cavity radius is about 22 m. The middle panel in Figure 12 shows the calculated nonlinear deformation region extent. The 3 red lines mark the boundaries of materials, i.e., from top to bottom, sediment, limestone, anhydrite and salt. Both limestone and anhydrite are strong materials and did not yield in the Salmon explosion simulation. Salt yielded out to a range of about 950 m, consistent with the spherical calculation (Rimer and Cherry, 1982). The weak sediment also yielded near the surface. The right panel in Figure 12 shows tensile cracking in salt and sediment. Cracks in salt are opened out to about 200 m from the explosion, and the sediment surface also shows some tensile cracking due to spall.

The calculated ground motions are compared with the Salmon data on the surface and in the salt layer in the near field in Figure 13. The stations are shown in the left panel in Figure 12. In Figure 13, the solid lines denote Salmon data and the dashed lines denote calculations. The bottom curves represent the radial components and the upper ones represent the vertical components. The two dimensional (2D) results are also in good agreement with the recordings at these locations. At the surface gauge (E-6-S), both the data and calculation show spall caused by the tensile wave reflected from the free surface, although the calculation shows somewhat earlier free fall of the uplifted surface than the data.

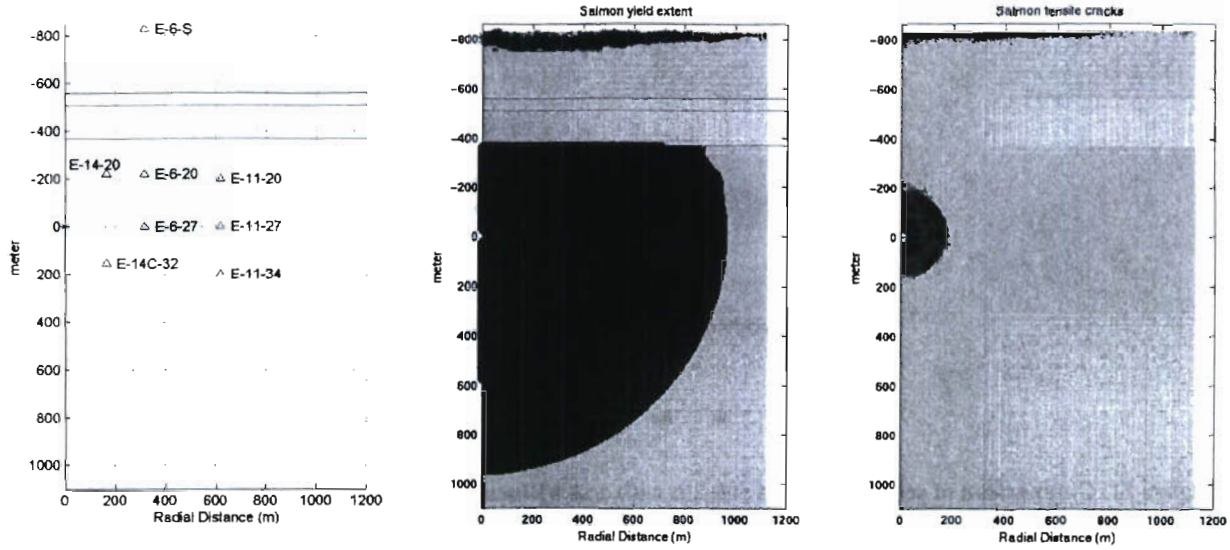

Figure 12. Left: Stations used for comparison of data and calculations. Middle: Nonlinear deformation distribution due to the Salmon explosion. Salt is yielded out to about 950 m, sediment top is partially yielded but limestone and anhydrite are not yielded. Right: Tensile crack distributions due to the Salmon explosion. Cracks open in the vicinity of the cavity within salt and near the free surface within sediment.

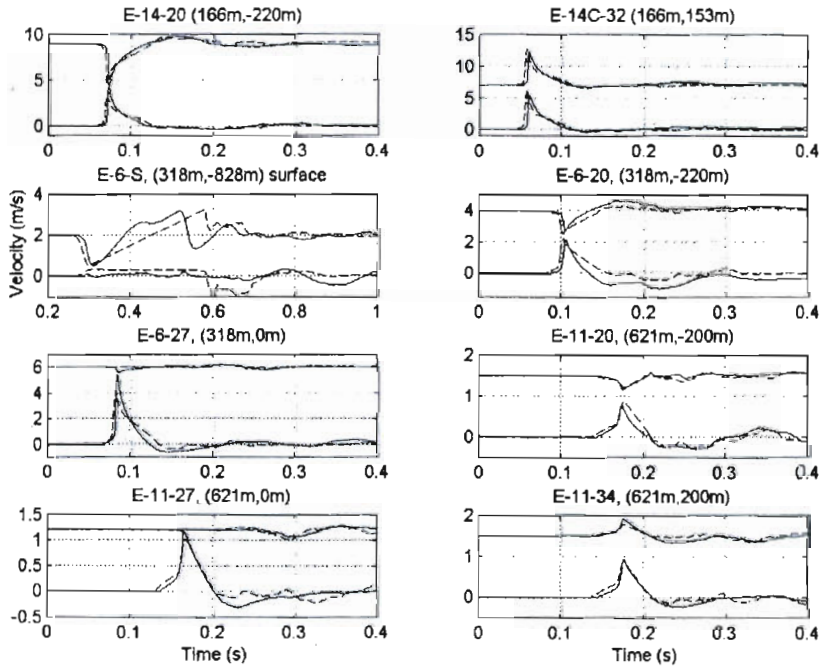

Figure 13. Comparison between the Salmon data and calculations. Spall is apparent from the –g slopes in the velocity waveform (E-6-S).

CONCLUSIONS AND RECOMMENDATIONS

In the first few months of this project, we have concentrated on numerical modeling of sources of shear waves from decoupled explosions. Specifically, we have modeled an explosion in an air-filled cavity offset from the center, an explosion in a cylindrical cavity, and explosion-generated hydrofractures. We plan to use these calculations together with analysis of data from decoupled explosions to assess which mechanisms are operating. We have also performed a detailed nonlinear finite difference calculation of the explosion Salmon, and plan to perform a detailed calculation of the decoupled explosion Sterling using the same model with a 17 m cavity (although the Salmon calculation generated a 22 m cavity, the observed cavity radius by the time Sterling was detonated was 17 m, probably because of creep during the intervening time).

In addition to the research program described above, we also plan to use data from Russian experiments in water-filled cavities (Murphy et al.; 2001). Although explosions in the water-filled cavities generate signals as strong as tamped explosions of the same yield, they are similar to air-decoupled explosions in that they generate little nonlinear deformation of the cavity—the stronger signal comes from the much higher pressure generated by the water-filled cavity compared to the air-filled cavity. These data sets are useful because they provide data in which the seismic signal from tamped and decoupled explosions are approximately the same size, reducing uncertainty that observed differences are caused by source size rather than tamped/decoupled differences.

REFERENCES

Latter, A. L., R. E. Lelevier, E. A. Martinelli, and W. G. McMillan (1961). A method of concealing underground nuclear explosions, *J. Geophys. Res.* 66: 2,929.

Murphy, J. R., D. D. Sultanov, N. Rimer, and B. W. Barker (2001). Seismic source characteristics of nuclear explosions in water-filled cavities, *Pure Appl. Geophys.* 158: 2,105–2,121.

Murphy, J. R. (1991). Free-field seismic observations from underground nuclear explosions, Explosion Source phenomenology, S. R. Taylor, H. J. Patton, and P. G. Richards (Eds). American Geophysical Union, pp. 25–33

Nilson, R, N. Rimer, and E. Halda (1991). Dynamic modeling of explosively driven hydrofractures, *J. Geophys. Res.*, 96: B11, 18,081–18,100.

Rimer, N., T. Barker, S. Rogers, J. Stevens, and D. Wilkins (1994). Simulation of seismic signals from partially coupled nuclear explosions in cylindrical tunnels, Defense Nuclear Agency report DNA-TR-94-136.

Rimer, N. and J. T. Cherry (1982). Ground motion predictions for the Grand Saline experiments, S-CUBED VSC-TR-82-25.

Stevens, J. L. (1980). Seismic radiation from the sudden creation of a spherical cavity in an arbitrarily prestressed elastic medium, *Geophys. J. R. Astr. Soc.* 61: 303–328.

Zhou, L. and D. G. Harkrider (1992). Wave fields from an off-center explosion in an embedded solid sphere, *Bull. Seism. Soc. Am.* 82: 1,927–1,955.